A Nanostructured Aptamer-Functionalised Black Phosphorus Sensing Platform for Label-Free Detection of Myoglobin, a Cardiovascular Disease Biomarker

DOI:
10.1021/acsami.6b06488

Document Version
Accepted author manuscript

A Nanostructured Aptamer-Functionalised Black Phosphorus Sensing Platform for Label-Free Detection of Myoglobin, a Cardiovascular Disease Biomarker

Vinod Kumar,[†1] Jack R. Brent,[†2] Munish Shorie,[1] Harmanjit Kaur,[1] Gaganpreet Chadha,[1] Andrew G. Thomas,[2] Edward A. Lewis,[2] Aidan P. Rooney,[2] Lan Nguyen,[2] Xiang Li Zhong,[2] M. Grace Burke,[2] Sarah J. Haigh,[2] Alex Walton,[3] Paul D. McNaughter,[3] Aleksander A. Tedstone,[3] Nicky Savjani,[3] Christopher A. Muryn,[3] Paul O'Brien,*[2,3] Ashok K. Ganguli,*[1,4] David J. Lewis,*[2,3] and Priyanka Sabherwal*[1]

[1]*Institute of Nano Science & Technology (INST), Habitat Centre, Phase-10, Sec-64, Mohali-160062, Punjab, India.*

[2]*School of Materials, University of Manchester, Oxford Road, M13 9PL, United Kingdom.*

[3]*School of Chemistry, University of Manchester, Oxford Road, M13 9PL, United Kingdom.*

[4]*Department of Chemistry, Indian Institute of Technology Delhi, Hauz Khas, New Delhi-110016, India*

ABSTRACT: We report the electrochemical detection of the redox active cardiac biomarker myoglobin (Mb) using aptamer-functionalised black phosphorus nanostructured electrodes by measuring direct electron transfer. The as-synthesised few layer black phosphorus nanosheets have been functionalised with poly-L-lysine (PLL) to facilitate binding with generated anti-Mb DNA aptamers on nanostructured electrodes. This aptasensor platform has a record-low detection limit (~0.524 pg mL^{-1}) and sensitivity (36 μA pg^{-1} mL cm^{-2}) towards Mb with a dynamic response range from 1 pg mL^{-1} to 16 μg mL^{-1} for Mb in serum samples. This strategy opens up avenues to bedside technologies for multiplexed diagnosis of cardiovascular diseases in complex human samples.

Keywords: Sensing, Heart Disease, Myoglobin, Aptamer, 2D Materials, Black Phosphorus.

Introduction

Two-dimensional (2-D) monolayer and few-layered materials have great potential due to their altered optoelectronic and mechanical properties as compared to their multi-layered bulk counterparts.[1] The archetypal 2-D material, graphene, has received enormous attention due to its high conductivity[2] and mechanical properties[3-4] which have been exploited in many applications.[5-6] Similarly, inorganic graphene analogues based on transition metal chalcogenides such as molybdenum disulfide (MoS_2)[7] have attracted attention due to their thickness-dependent semiconducting properties.[8] The utility of these nanomaterials, however, are limited by intrinsic shortcomings, such as lack of a bandgap in graphene[9] and relatively low carrier mobility in MoS_2,[10] all of which has motivated a continued search for new 2-D materials. Recently monolayer black phosphorus (BP), also known as 'phosphorene', has emerged as an important member of this family of 2-D materials.[11] In monolayer phosphorene, each phosphorus atom forms bonds with three neighbouring phosphorus atoms to give a puckered honeycomb structure. Phosphorene and few-layer black phosphorus nanosheets can be synthesised by mechanical exfoliation of black phosphorus[11] or by liquid-phase exfoliation of black phosphorus in *N*-methyl-2-pyrollidone (NMP)[12-13] and other organic solvents.[14-15] BP exhibits a direct and tuneable band gap that is dependent on the number of layers (bulk: 0.3 eV, monolayer ca. 1.3 eV).[16-18] Monolayer BP has a measured free carrier mobility (ca. 1000 cm^2 Vs^{-1})[11] that is superior to MoS_2 (ca. 100 cm^2 Vs^{-1}).[10] Phosphorene also exhibits other fascinating and useful properties, including anisotropic electrical conductivity and optical response,[11, 16, 19] which distinguishes it from other 2-D materials such as graphene, and metal chalcogenides.

Cardiovascular diseases account for ca. 30% of adult deaths in the age group of 30-70 years, which is greater than the combined mortality rate from all types of cancer.[20] The ability to foresee cardiac pathology is therefore of utmost concern to clinicians. Several potential cardiac biomarkers have attracted attention because of

ATCCAGAGTGACGCAGCACAACGTGCAAATTATACCTGTTTTCCCCTTTTCCTACAAGTGCTATGGACACGGTGGCTTAGT

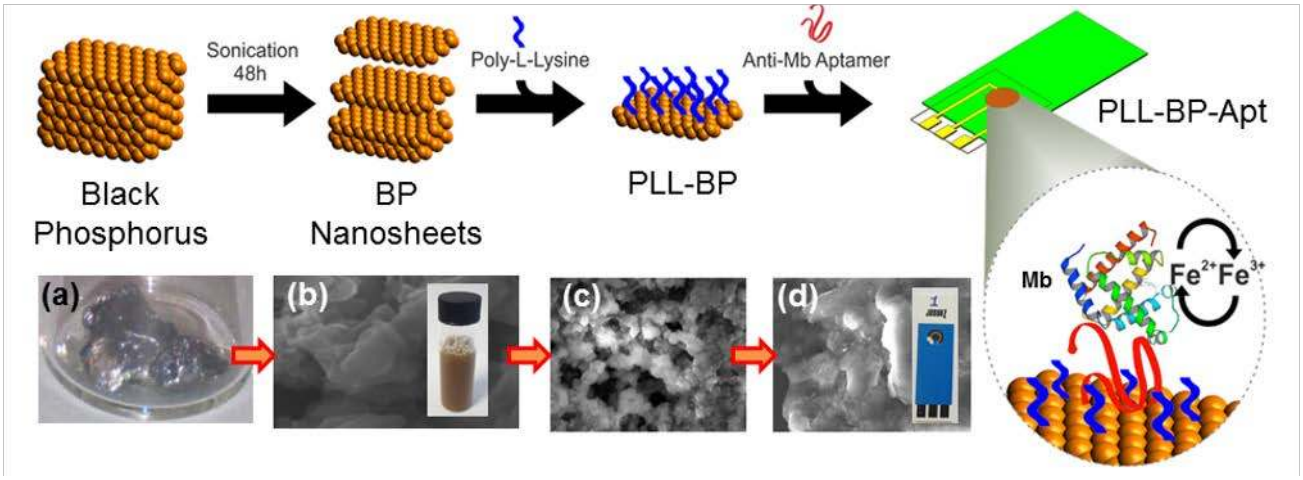

Figure 1. Schematic representation of workflow for the liquid phase exfoliation of BP nanosheets and their surface modification for bio-interface development on an electrode for Mb detection. The panels shown below the workflow scheme depict images of the real colloid, the assembled sensor and representative secondary electron SEM images taken at each stage. (a) Bulk black phosphorus prior to liquid-phase exfoliation. (b) Representative secondary electron SEM image of exfoliated few-layer BP from aqueous 1% *w/v* Triton X-100 solution. Inset: photograph of the stable colloid. (c) SEM image of few-layer BP functionalised with PLL. (d) SEM image of few-layer BP functionalised with PLL and anti-Mb aptamer (PLL-BP-Apt). Inset: photograph of the sensing device on a screen-printed electrode as used for sensing Mb in this study. The DNA sequence of the SELEX derived anti-Mb aptamer is shown above.

their ability to predict future cardiovascular events.[21] Serum cardiac markers, especially myoglobin (Mb), plays an important role in clinical diagnosis; an increased Mb level indicates myocardial damage.[22] Detection of elevated levels of Mb has become a gold-standard for diagnosis in cases of acute myocardial infarction (AMI); Mb is released in the blood within 4-5 h after an AMI episode,[23] with the expression level in plasma serum increasing up to 600 ng mL^{-1} after AMI, over 3 to 6 times above the normal level expressed in healthy patients.[24] The early and rapid diagnosis of AMI is extremely important for a positive prognosis,[25] yet current Mb detection methodologies rely on analysis in centralised laboratories which are often costly and time-consuming.[26] Thus, development of proficient point-of-care (POC) diagnosis based on biochemical sensors paves the way to rapid cardiac disease management.

Affinity-based assays which use specific antibodies or nucleic acid (DNA or RNA) aptamers for a target protein or small molecule offer a facile approach to biosensing with potential for high selectivity and sensitivity.[27] Nucleic acid aptamers have been utilised as superior alternatives to antibodies due to their smaller size, molecular flexibility, *in-vitro* screening and ease of chemical modifications which allows them to be the quintessential candidate for biosensing platforms.[28-29] Recently, the use of 2D materials has been established in the sensitive detection of biomolecules from blood samples.[30-31] The combination of nucleic acid aptamers with nanomaterials is promising in the development of novel diagnostic platforms for clinically important biomarkers.[32] 2-D nanomaterials in combination with aptamers offer the possibility of creating biosensing platforms with enhanced selectivity and unprecedented sensitivity compared with available conventional detection methods. In the present study, the exfoliation of black phosphorus to give stable few-layer BP in aqueous medium using a surfactant-mediated approach has been developed. The characterised BP nanosheets were modified with cationic polymer poly-L-lysine (PLL) which functions as a linker for further biomolecular interactions with the underlying BP. Theoretical calculations predict this interaction occurs through the nitrogen atoms on PLL. Negatively charged DNA aptamers for Mb were selected from the pool of random-sequence oligonucleotides using the systematic evolution of ligands by exponential enrichment (SELEX) method,[33] and these were immobilised on the nanosheets *via* Coulombic interactions between PLL and DNA. These nanostructured platforms were employed in electrochemical-based sensing for the qualitative and quantitative detection of the cardiac disease biomarker, Mb (Fig. 1). The developed aptasensor showed high sensitivity and specificity for Mb and has singular potential in POC diagnosis for cardiac disease management.

Experimental Section

Materials. Black phosphorus (BP) was purchased from Smart Elements (Austria). Triton X-100, poly-L-lysine (PLL), myoglobin (Mb), haemoglobin (Hb), bovine serum albumin (BSA), DNA library 5'-ATCCAGAGTGACGCAGCA-(N45)-TGGACACGGTGGCTTAGT-3' and the designed primers: 5'-FITC-ATCCAGAGTGACGCAGCA-3' and 5'-biotin-ACTAAGCCACCGTGTCCA-3' were procured from Sigma-Aldrich.

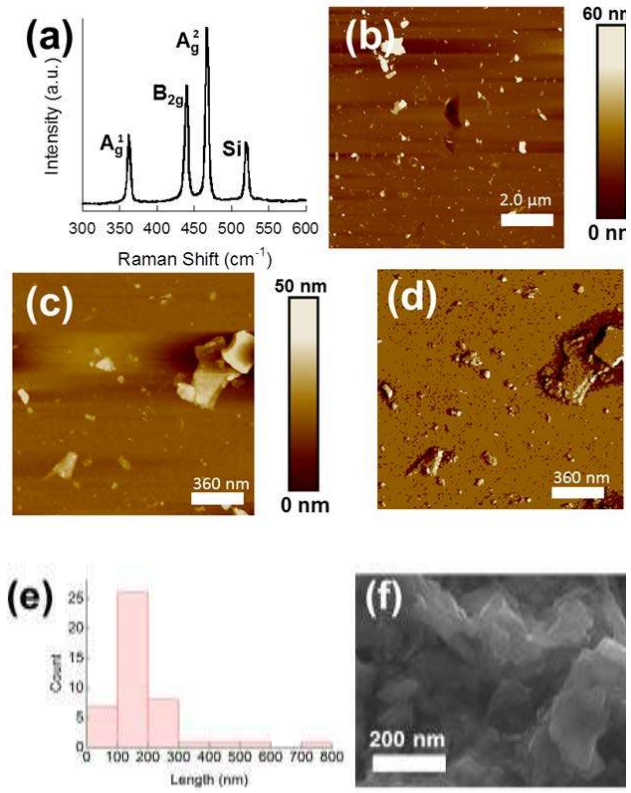

Figure 2. Characterisation of liquid-phase exfoliated BP nanosheets. (a) Raman spectrum of exfoliated (in aqueous 1% *w/v* Triton X-100 solution) few-layer BP on SiO_2/Si substrate showing the characteristic Raman bands at 362 cm^{-1}, 440 cm^{-1} and 465 cm^{-1} assigned to the A^1_g, B_{2g} and A^2_g phonon modes. (b) Wide-area atomic force microscopy height profile image of few-layered BP sheets SiO_2/Si substrate. (c) Narrow-area atomic force microscopy height profile image of few-layered BP on SiO_2/Si substrate. (d) DMT elastic modulus map of the area imaged in (c). Dark halos observed around the flakes were revealed to be surfactant by low voltage EDX spectroscopy (see Supporting Information for further details). (e) Flake lateral length histogram of few-layered BP. (f) Secondary electron SEM image (6 kV) of few-layer BP. The scale bar represents 200 nm.

Instrumentation. Raman spectra were measured using Renishaw 1000 Micro-Raman System equipped with a 514 nm laser operating at 1 mW. Atomic force microscopy (AFM) was performed using Bruker Multimode 8 instrument in PeakForce QNM mode using silicon nitride cantilever tip. Transmission electron microscope (TEM) imaging, high angle annular dark field (HAADF) scanning transmission electron microscope (STEM) imaging, and energy dispersive X-ray (EDX) spectrum imaging were performed using a FEI Tecnai F30 TEM operated at 300 kV. HAADF STEM and electron energy loss spectroscopy (EELS) was performed using a probe side aberration corrected FEI Titan G2 80-200 S/TEM "ChemiSTEM™" instrument operated at 200 kV, with a convergence angle of 18.5 mrad, a HAADF inner angle of 54 mrad and a probe current of ~200 pA. For the electrochemical studies, screen printed electrodes (SPE, TE 100, CH Instruments USA) were used and the measurements were carried out on CH660 electrochemical workstation. Optical absorption measurements were performed with a Shimadzu UV 1800 instrument. Scanning electron microscopy (SEM) was performed using a Zeiss Sigma VP. Low voltage energy dispersive X-ray (EDX) spectroscopy was performed on a Zeiss Merlin SEM equipped with a windowless EDX system (X-Max Extreme, Oxford Instruments). Compared with conventional detector systems, it has low noise electronics, high resolution 100 mm^2 SDD sensor, large solid angle and high sensitivity. EDX spectra and the respective images were analysed using AZtec software. X-ray photoelectron spectroscopy (XPS) was performed using a Kratos Axis Ultra system.

Black phosphorus nanosheet synthesis by surfactant-assisted liquid phase exfoliation. BP nanosheets were synthesised using an aqueous surfactant solution (1 mg mL^{-1} prepared in Triton X-100 and deionised water) which was thoroughly degassed before use. In a sealed vial, this surfactant solution (15 mL) was added to BP (100 mg, 3.2 mmol) and the vial was flushed with argon, closed and sealed with Parafilm®. Suspensions were sonicated in an Elmasonic P 70 H bench-top ultrasonic bath (820 W across four horns) operating at 37 kHz and 30% power. The temperature of the bath was maintained at 25 °C throughout via the use of a home-made cooling coil. After 36 h the dispersions were centrifuged at 1500 rpm for 45 min and the top 10 mL of the suspension was removed. Further 10 mL of surfactant solution was added to the remaining dispersion and the sediment mixture was sonicated again for 12 h under the same conditions. The dispersion was centrifuged and the supernatant was added to the previously collected dispersion.

Spectroscopic and microscopic characterisation of black phosphorus nanosheets. The dispersions of black phosphorus nanosheets were spin-coated at 2000 rpm onto 300 nm silicon-coated SiO_2 (SiO_2/Si) substrates using an Ossila spin coater for Raman and AFM analysis. For (S)TEM) imaging samples were prepared by drop casting 15 µl of dispersions onto gold-coated carbon Quantifoil® grids with a hole size of 1.2 µm. Deionised water was used to wash off the excess solvent from the grids. Samples were immediately transferred to the microscope for imaging after preparation, to minimise the photo-oxidative degradation. EEL spectrum images were acquired from 20 BP flakes with large lateral dimensions (>200 nm). Measurements of t/λ (where t is the sample thickness and λ is the mean free path of inelastic electron scattering) were extracted from the spectrum images using Gatan Digital Micrograph software.

Synthesis and characterisation of PLL functionalised black phosphorus nanosheets. The as-synthesised dispersion of exfoliated BP nanosheets in aqueous Triton-X-100 was concentrated and subsequently centrifuged at 3000 rpm to remove the surfactant. The resulting sediment was re-dispersed in aqueous solution of PLL (1 mg mL^{-1}) which was stirred for 1 h followed by incubation for 12 h at 4°C. The resulting PLL-BP dispersion was characterised by Raman spectroscopy, zeta potential and contact angle measurements to evaluate the interaction of PLL with exfoliated BP.

Generation of specific anti-Mb aptamer using modified systematic evolution of ligands by exponential enrichment (SELEX). The specific DNA aptamers were screened from a pool of oligonucleotides with a random region of 45 nucleotides flanked by constant primer-binding region of 18 nucleotides by using a SELEX method.[27] Briefly, Mb (10 μg mL^{-1} prepared in 50 mM carbonate buffer pH ~9.6) was immobilised by incubating overnight at 4°C on microtiter plates, onto which 10^{14} molecules of ssDNA library were exposed. Harvested DNA binders were PCR amplified and partitioned to produce ssDNA. The generated DNA was subjected to iterative cycles of exposure to the immobilised Mb followed by elution, PCR amplification and partitioning to screen highly specific DNA aptamer with a dissociation coefficient (K_d) of 65 pM (Supporting Information ST1, ST2).

Mb detection on PLL-BP nanostructured electrodes. As-prepared PLL-BP (3 μL) was drop-casted onto the working area of a screen-printed electrode (SPE) and dried at 50°C for 2 h under argon. The electrochemical performance of the PLL-BP modified electrodes were studied with cyclic voltammetry (CV) measured in 5.0 mM potassium ferricyanide/potassium ferrocyanide solution (prepared in 100 mM phosphate buffered saline, PBS) at a sweeping potential ranging from -1 to +1 V with a scan rate of 100 mV s^{-1}. For assay development, 1 μg of anti-Mb DNA aptamer (200 μg mL^{-1} stock prepared in 10 mM Tris buffer supplemented with 150 mM NaCl and 5 mM $MgCl_2$, pH ~7.2) was drop-casted over PLL-BP modified electrodes. The CV responses of the fabricated aptasensor were recorded at different concentrations of Mb ranging from 1 pg mL^{-1} to 16 μg mL^{-1}.

Results and Discussion

Surfactant-assisted liquid phase exfoliation and characterisation of few-layer BP nanosheets. The exfoliation of BP has been previously reported in several organic solvents[12–15] including *N*-methyl-2-pyrollidone (NMP), *N*-cyclohexyl-2-pyrollidone (CHP), dimethyl sulfoxide (DMSO) and *N,N*-dimethyl formamide (DMF) all of which are biologically incompatible. This study reports the use of aqueous medium to afford exfoliated BP nanosheets, which unlocks the direct application of the material in biological systems.

BP nanosheets were synthesised by ultrasonic exfoliation of a BP crystal in water containing 1% *w/v* of Triton X-100 (a non-ionic surfactant). A turbid brown-coloured solution was produced (Supporting Information, ST3 and Fig. 1 for an example of the Triton X-100 sol). Raman spectroscopy of the exfoliated BP nanosheets revealed bands at 362 cm^{-1}, 440 cm^{-1} and 465 cm^{-1} assigned to the A^1_g, B_{2g} and A^2_g optical phonons of few-layer BP (Fig. 2a). Atomic force microscopy was used to assess the thickness of nanosheets (Fig. 2b,c,d), up to 60 nm in height. The nanosheets were also imaged using modulus mapping which showed that these sheets share a modulus similar to the silicon substrate. However, dark halos were observed around the sheets, which from low voltage EDX spectroscopy measurements is revealed to be surfactant wrapped around the immobilised nanosheets. Scanning electron microscopy of the flakes revealed them to be fairly monodisperse in length (ca. 100 – 200 nm, Fig. 2e) and electron-transparent at 6 kV (Fig. 2f).

The nanosheets were further characterised by bright field TEM and HAADF STEM imaging (Fig. 3a, c). Selected area electron diffraction (SAED) of an isolated nanosheet (Fig. 3b) demonstrated the crystallinity of the structure, with *d*-spacings of 2.6, 1.8, 1.7, 1.6 and 1.3 Å which were assigned to the (111), (121), (024), (202) and (204) reflections of black phosphorus. EDX spectroscopy of the nanosheets further confirmed the major element present is phosphorus (Supporting Information, ST4). EDX spectrum imaging of the nanosheets (Fig. 3d) confirms undoubtedly that the phosphorus signal is co-localised with the spatial location of the nanosheet in the HAADF STEM image.

The thickness of the BP nanosheets was also calculated using electron energy loss spectroscopy (EELS) which provides an alternative method for local thickness estimation by determining the proportion of inelastic scattering. Although accurate thickness can also be obtained for few layer flakes using electron diffraction data[34] this approach generally requires flakes with uniform thickness and lateral dimensions ≥200 nm, and hence was found to be unreliable as liquid exfoliated flakes often have regions of restacked material, non-uniform thicknesses ≥10 nm and small lateral dimensions.

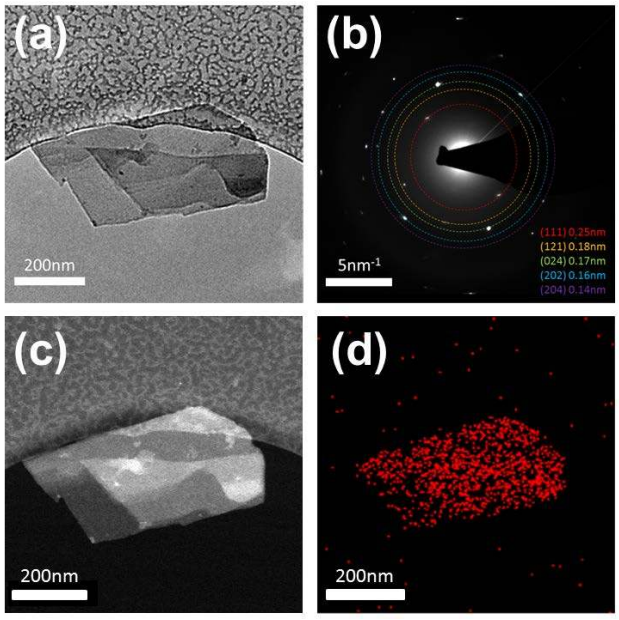

Figure 3. Characterisation of an exfoliated BP nanosheet of dimensions ca. 600 nm × 400 nm, aspect ratio ca. 1.5, by TEM at 200 kV. (a) Low magnification TEM image of a BP nanosheet. (b) selected-area diffraction pattern taken from the same region as in (a). (c) HAADF STEM image. (d) EDX spectrum image of the same BP nanosheet as in (c), showing the morphology and the distribution of phosphorus within the sheet. The flake shown here is typical in terms of aspect ratio, crystallinity, elemental analysis and morphological features.

Flake thickness (t) was calculated using an estimated λ (mean free path of inelastic electron scattering) value of ~144.9 nm, calculated by the Iakoubovskii method.[35] Typically the individual flakes were found to include regions of different thickness (Fig. 4) which are partly due to re-stacking, with smaller flakes aggregating on the surface of larger flakes either in solution or during the drying process. Step changes in thickness were widely observed within the flakes, often with the thinnest regions found at the edges and the thickness increasing towards the centre of the flake (Fig. 4), suggesting that the flakes themselves also contain terraces of different thickness features which are frequently observed in liquid exfoliated two-dimensional materials.[15, 36] In order to take into consideration the range of thicknesses encountered within an individual spectrum image both the thickest and thinnest measured region of each flake analysed were recorded and the mean thickness of the flake was estimated as an average of these two values (Supporting Information, ST5, Table T1). The mean thickness of 20 flakes was measured to be ~19 nm with the lateral dimensions >200 nm, which gives an estimated width:height aspect ratio of >10:1. The thinnest areas recorded are 4-6 nm and as the monolayer is ~ 0.9 nm thick, this suggests that no monolayer regions were encountered for the large flakes considered in this EELS study, but that the thinnest regions analysed have thicknesses of 5 or more atomic layers and the thickest regions encountered correspond to >40 atomic layers. Monolayer surface steps and isolated terraces were observed on the larger flakes studied here, suggesting that monolayer material may exist for flakes with smaller lateral dimensions.

Surface modification of black phosphorus nanosheets with poly-L-lysine. The exfoliated BP nanosheets were modified at their surface with PLL to develop an interface for DNA aptamer functionalisation for specific Mb sensing. The resulting PLL-BP dispersion was characterised by various microscopic and spectroscopic techniques to evaluate the surface modifications. Low magnification SEM micrographs of PLL-BP on the electrode surface showed an increase in surface roughness (supporting information ST6, S4a-c) and a uniform coverage with phosphorus atoms was recorded in the elemental mapping (supporting information ST6, S4d). High magnification SEM imaging performed by modifying Si/SiO_2 surface with nanosheets indicated clearly visible smooth surfaces (Supporting Information, ST6, Fig. S4e-h), however the surface roughness is increased upon interaction with PLL. When DNA is immobilized over PLL-BP, the surface is completely covered and further addition of Mb led to an altered morphology. Analysis of Raman spectra revealed a red shift in the characteristic bands of PLL-BP conjugate from 362 cm^{-1}, 440 cm^{-1} and 465 cm^{-1} (unmodified) to 359 cm^{-1}, 433 $cm^{-1}$and 460 cm^{-1} (PLL modified) which again are assigned to the A^1_g, B_{2g} and A^2_g optical phonons respectively (Supporting Information, ST7, Fig. S5).

Upon functionalisation of BP with PLL, the value of zeta potential was changed from -23.4 mV to +13.5 mV. The characterised PLL-BP (3 µL of 1 mg mL^{-1} of colloid) was transferred onto the working area of a screen printed electrode (SPE) and further characterised. The sensor surface characteristics play an important role towards the efficient interactions of the immobilised bio-receptors with the target analyte. The modified sensor surface characteristics (hydrophilicity/hydrophobicity) were studied by contact angle measurements which showed a decrease in mean contact angle (117.5° to 84.1°) in comparison to a bare electrode, indicating an increase in hydrophilicity. We attribute this to the sensor modification with PLL-BP having two amino groups present at α-carbon and ε-carbon along with one carboxylate group ($-COO^-$)(Supporting Information, ST9, Fig. S7). The interaction of PLL with the BP surface was further investigated with DFT calculations (see Supporting Information ST23 for full details).

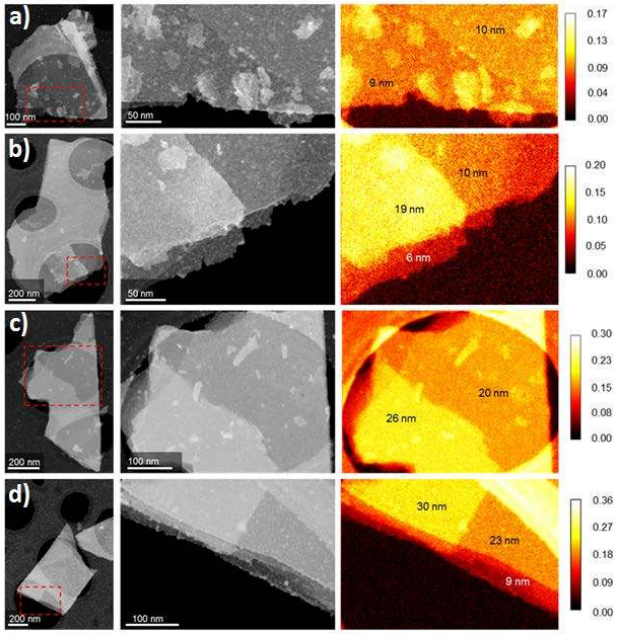

Figure 4. EELS thickness analysis of exfoliated few layer BP. (a), (b), (c), (d), Four typical BP flakes are shown in low magnification high angle annular dark field (HAADF) STEM images in the left column; the dashed red box indicates the region studied by EEL spectrum imaging. The middle column shows a higher magnification HAADF image of this region and the right column contains maps of t/λ values extracted from the EEL spectrum image. Thickness values (calculated using λ=144.9 nm) are superimposed on the t/λ maps.

Bio-interface development using DNA aptamers. Appropriate DNA aptamers which bind selectively to Mb were selected using SELEX by exposing the target molecule (Mb) immobilised on a microtiter plate to a single stranded DNA (ssDNA) library as reported previously.[33] Liquid chromatography was used to assess the binding of developed aptamer with Mb by monitoring absorbance at 260 nm, 280 nm and 409 nm (Supporting Information, ST10, Fig. S8). The biomolecular interactions lead to the shift of the molecular weight of standard Mb from 16.7 KDa to 41.2 KDa suggesting its interaction with the screened aptamer having molecular weight 24.5 KDa. The characterised SELEX generated anionic aptamer was con-

jugated to the cationic PLL-BP by Coulombic interactions, thus creating a stable bio-interface on PLL-BP as per the mechanism summarised in Fig. S9. The PLL-BP nanostructure was further characterised by zeta potential measurement, where a shift of 25.6 mV in zeta potential was observed with respect to PLL-BP, which is ascribed to the electrostatic interactions of available positively charged $-NH_3^+$ groups of PLL with negatively charged DNA phosphate backbone leading to partial charge neutralisation (Supporting Information ST8, Fig. S6). Raman spectroscopy further supported this by revealing a comparative shift in characteristic Raman bands of PLL-BP after DNA interactions (Supporting Information, ST7, Fig. S5). The contact angle measurements of PLL-BP aptasensor platform reveals a decrease in contact angle value to ~84.1° when the anti-Mb DNA aptamer was immobilised on PLL-BP nanostructured electrodes which we ascribe to its increased hydrophilicity from hosting essentially two types of charged polymers (PLL, DNA) (Supporting Information ST9, Fig. S7).

Monitoring the layer-by-layer assembly of nanostructured aptasensor electrodes with X-ray photoelectron spectroscopy (XPS). XPS gave further insight on the layer-by-layer bio-functionalisation strategy that we adopted (Fig. 5). The peaks at lower binding energies in the XPS spectra arise due to BP and the broader peak is due to oxidised BP (PO_x) and phosphorus hydroxide ($P(OH)_x$) species (Fig. 5). On fitting only one doublet, the broader full width at half maximum (FWHM) of the peaks on the $PO_x/P(OH)_x$ feature suggest that these are likely due to be due multiple components. Since it is impossible to know the precise composition of the oxidised BP, any attempt to fit multiple components would be meaningless. Following exfoliation of the BP with Triton X-100 the PO_x component is dominant, yet this may be expected as the sol will always contain an 'equilibrium' amount of free phosphate that will dominate over the BP peak. It is likely that phosphate adsorbs to the flakes after drop casting etc. and we cannot separate this effect from the amount of 'natural' degradation on the surface of the flakes. The C 1s peak of the Triton treated BP (Fig. 5, X1) can be fitted with two components; one at 285 eV, due to C-C/C-H and a second one at a binding energy of 286.6 eV, which is attributed to either C-O-C in the polyethylene glycol component or the surfactant. A small peak is also observed at ~289 eV, which arises from C-OH species, also found in the surfactant. The C 1s peak is also likely to have some contribution due to the presence of adsorbed adventitious hydrocarbon since the samples have been exposed to atmospheric conditions prior to XPS analysis. A broad N 1*s* peak was recorded from this sample. The origin of the N 1*s* signal is unknown and is observed in all samples subjected to XPS analysis. Upon interaction with PLL (Fig. 5, X2) a second N 1*s* peak is observed, which is assigned to the amine in the lysine. The BP peak is enhanced relative to the PO_x peak, which suggests large amount of adventitious phosphate from solution degradation being washed away during functionalisation with PLL. Despite using the same data acquisition time it is clear that the P 2*p* signal is decreased relative to C and N 1s signals, as the noise level increases. The higher binding energy feature (286.6 eV) in C 1s spectrum increases after PLL adsorption since C-N has a similar binding energy to C-O-C from the ethylene glycol. In addition, the feature at 289 eV increases slightly in intensity as more C-OH will be present from PLL. Addition of DNA (Fig. 5, X3) gives rise to very little change

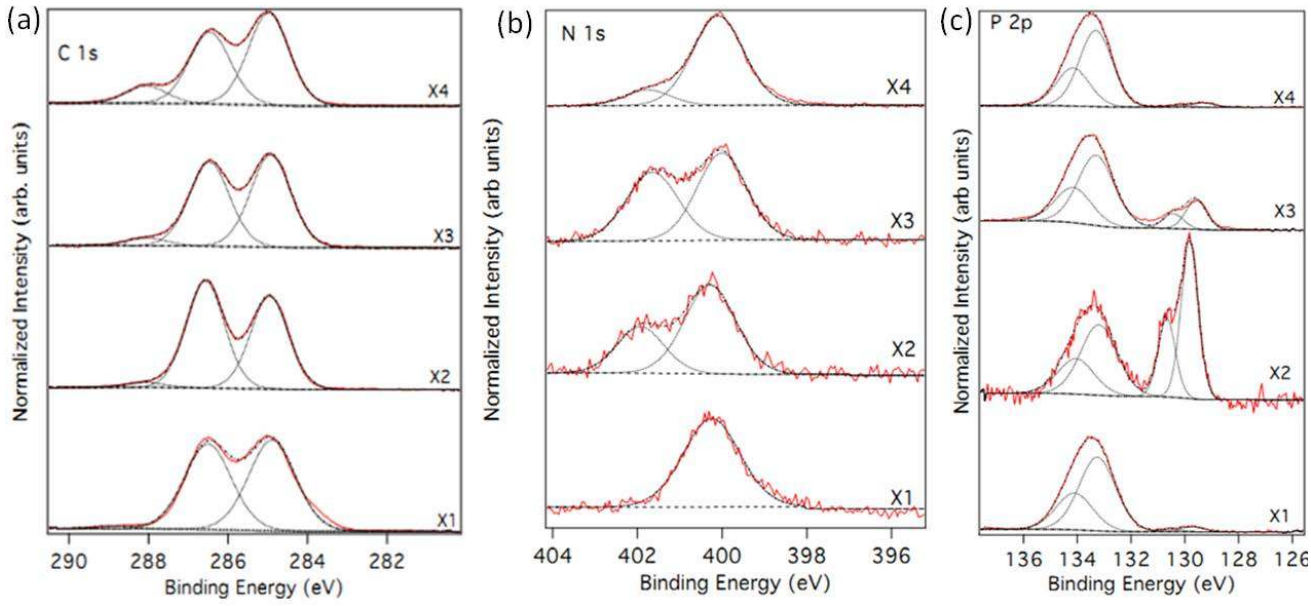

Figure 5. X-ray photoelectron (XPS) spectroscopy monitoring the layer-by-layer assembly of the aptasensor. (a), (b) and (c) show C1*s*, N1*s* and P2*p* comparative XPS spectra of BP nanosheets (X1), PLL-BP (X2), PLL-BP-Apt (X3) and PLL-BP-Apt-Mb(X4) respectively.

in C 1s peaks and the assignment of these peaks is as for PLL. The P 2p spectrum is dominated again by PO_x, in part due to the DNA backbone signal. Again without prior knowledge of the precise proportion of the P-oxides and hydroxides and DNA derived P-O components it is impossible to meaningfully fit the PO_x spectra. As expected the signal due to amine N increases slightly upon addition of the DNA from the nucleobases. Finally addition of Mb (Fig. 5, X4) leads to almost complete suppression of the BP-derived P 2*p* signal (since the protein overlayer becomes comparable to the sampling depth of XPS, ca. 10 nm). A strong PO_x signal however, arises from the bound DNA. In summary XPS allowed us to observe the layer-by-layer assembly of the aptasensor.

Myoglobin detection on the nanostructured aptasensor electrodes. The modified nanostructured electrodes were employed for the detection of Mb by cyclic voltammetry. The PLL-BP nanostructured electrodes showed a significant increase in current response (~1.3 mA) in comparison to the bare electrode (~0.64 µA) as shown in Fig. 6a. The enhanced electrochemical response of the material is attributed to BP's inherent redox properties which show a significant oxidation peak at ~0.6V (*vs* AgCl) corresponding to the oxidation of P^0 to P^{5+} species.[37] In our study, the electro-active area of the PLL-BP modified electrode was estimated to be ~13.8 mm^2 using the Randles-Sevcik equation (Supporting Information, ST13). A slight decrease in current signal (0.28 mA) with a small shift in the cathodic peak potential (0.11 V) was observed which is ascribed to the immobilisation of DNA aptamers on PLL-BP functionalised SPE (Fig. 6a). The PLL-BP SPE showed a diffusion controlled electron transfer, evidenced by the linear increase (1.2 to 2.1 mA) in the cathodic peak intensity with increasing scan rate (25 – 300 mV s^{-1}) (Fig. 6b). In addition, the redox peak current increases linearly with the square root of the scan rate, indicating that the redox reaction is controlled by a semi-infinite linear diffusion revealing a rapid electron transport nature.[38] The observations were further supported by scan rate (25-300 mV s^{-1}) dependent electrical impedance spectroscopic (EIS) studies (Supporting Information, ST14). The real and imaginary part of the EIS spectra (Supporting Information, Fig. S11) represents Nyquist plots (Z' vs. Z'') for BP-modified SPE using 10 mM $Fe(CN)_6^{3-/4-}$ as the electrolyte. The Randles equivalent circuit model has been used to fit the experimental data where R_{sol} is electrolyte resistance, R_{ct} is charge transfer resistance, C_{dl} is double layer capacitance and W is the

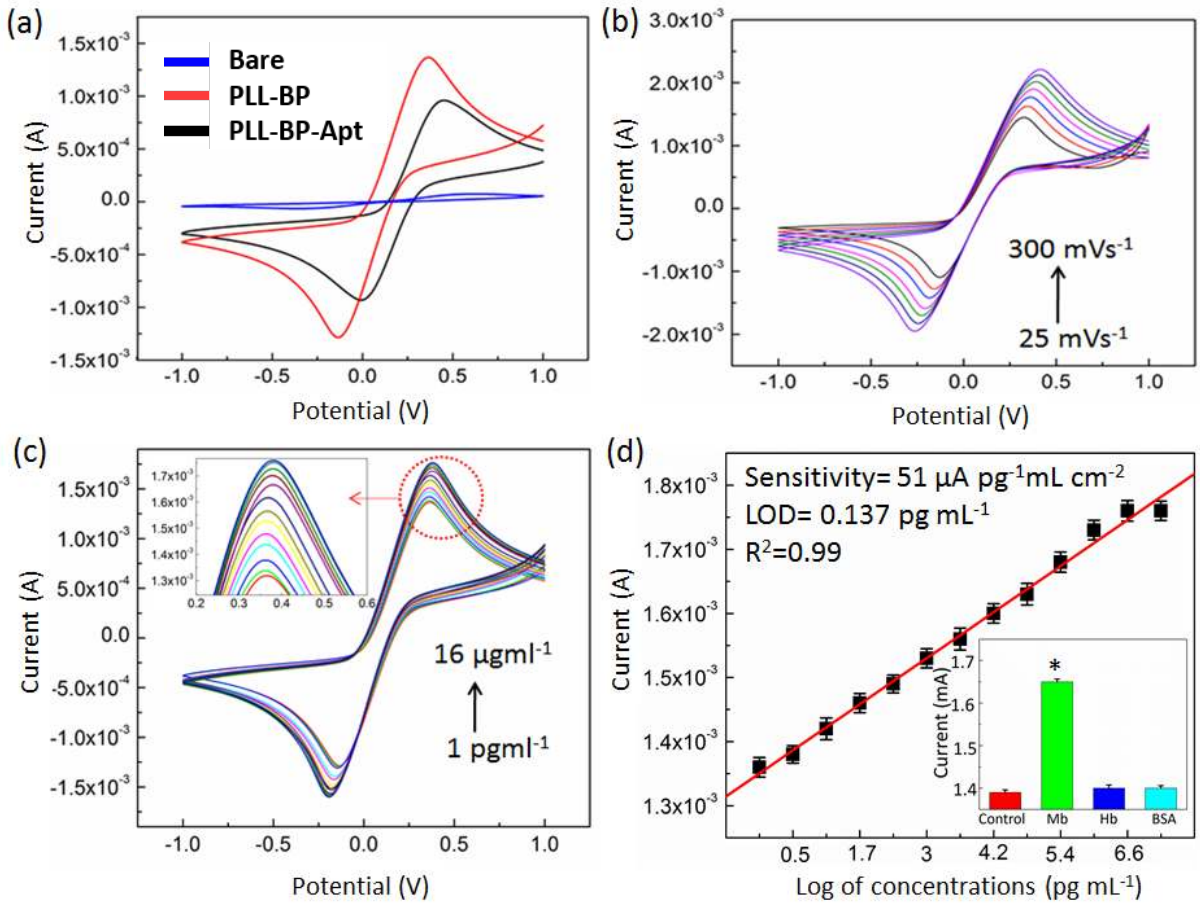

Figure 6. Sensing platform performance. (a) Electrochemical response curve of bare, PLL-BP and PLL-BP-Apt modified electrodes using 5mM potassium ferricyanide/potassium ferrocyanide solution (prepared in 100 mM PBS) at a sweeping potential ranging from -1 to +1 V with a scan rate of 100 mV s^{-1}. (b) CV scans of PLL-BP nanostructured electrode, recorded at different scan rates from 25 to 300 mVs^{-1}. (c) Current response curves at varying concentration of Mb measured on PLL-BP nanostructured aptasensor. Inset shows the zoom in area of redox peak of Mb obtained. (d) Calibration plot for Mb at different concentrations. Every point in the graph represents the mean of three successive measurements (n=3) at each concentration. Inset shows the cross reactivity profile of developed sensor with a structurally related protein (Hb) and a non-related protein (BSA).

Warburg impedance. The values of equivalent circuit elements were also calculated. The charge transfer process was then ascertained by measuring the charge transfer resistance (R_{ct}) at the electrode/electrolyte interface. The value of R_{ct} for the nanostructured electrode was found to be ~33.3 Ω at 25 mV s^{-1} and decreases with increasing scan rate which depends on the dielectric and insulating features at the electrode/electrolyte interface. The electrochemical stability of PLL-BP SPE was tested by repeated cyclic scanning (100 cycles), which showed insignificant change in the peak currents (Supporting Information, ST15, Fig. S12). DNA aptamer was drop-casted on the working area of the PLL-BP modified electrode to a final concentration of 1 µg/electrode in order to uniformly cover the electrode surface (Supporting Information ST16, Fig. S13). A series of Mb standard concentrations (prepared in phosphate-buffered saline, 10 mM, pH 7.4) were exposed to the nanostructured aptasensor and the resulting cyclic voltammogram presented a concentration dependent reduction peak at a potential of -0.5 V due to the redox property of Mb analyte as shown in Fig. 6c. In its native form, Mb contains a heme group as an active site with and iron(II) centre which can be oxidised directly at the electrode surface to iron(III) by a one-electron transfer mechanism as per the following equation:[39]

$$\text{Mb-Fe(II)} \longleftrightarrow \text{Mb-Fe(III)} + e^-$$

The platform provides the label free electrochemical detection of Mb on aptamer functionalised PLL-BP electrodes by direct electron transfer. The calibration plot for Mb at different concentrations showed a strong linear trend (R^2=0.99) indicating a concentration dependent current signal response of the DNA aptamer 2-D sensing platform. The assay showed excellent sensitivity (51 µA pg^{-1} mL cm^{-2}), in the dynamic response range between 1 pg mL^{-1} to 16 µg mL^{-1} for Mb with a limit of detection (LOD) of ~0.137 pg mL^{-1} (Fig.6d). The cross-reactivity of the aptasensor to a structurally related protein, haemoglobin (Hb) and another non-related ubiquitous plasma protein, bovine serum albumin (BSA) (1µg/mL each) showed a strong preference for the binding of Mb to the PLL-BP-Apt functionalised electrode (inset of Fig. 6d). As controls, the sensor was checked for signal response with the various modifications in this paper, namely PLL; PLL-Apt; PLL-Apt-Mb along with BP exfoliated in Triton-X-100; BP-Apt, BP-Apt-Mb. No significant current response change indicated the high specificity and sensitivity of the developed aptasensor imparted by the immobilised anti-Mb aptamer onto PLL-BP nanostructured electrodes (Supporting Information, ST17, Fig. S14). The assay was validated against serum samples spiked with varying concentrations of Mb; the aptasensor showed high sensitivity (36 µA pg^{-1} mL cm^{-2}) with a LOD of ~0.524 pg mL^{-1} for Mb in serum samples (Supporting Information, ST18 Fig. S15). Furthermore, the signal response of the BP nanostructured aptasensor was compared with reduced graphene oxide (rGO) under same set of conditions used for Mb sensing (Supporting Information ST19, Fig. S16). The rGO based aptasensor shows a detection limit of ~1.3 ng mL^{-1}, with a sensitivity of 10 µA ng^{-1} mL cm^{-2} with a dynamic response range of 4 ng mL^{-1} to 16 µg mL^{-1} for Mb spiked in serum which are both inferior to the reported few layered black phosphorus-based Mb sensor.

To assess aptasensor stability, 6 identical PLL-BP-Apt sensors were investigated by observing the current response at different time intervals i.e. on 0^{th}, 1^{st}, 3^{rd}, 7^{th}, 14^{th} and 21^{st} day with 256 pg mL^{-1} concentration of Mb both in PBS and in serum samples. The results of these studies indicated no significant decrease in the current (within 5%) after 21 days for both Mb in PBS and in serum, revealing the excellent storage stability of the developed aptasensor (Supporting Information, ST20, Fig. S17). Post-sensing XPS analysis of the developed sensor demonstrated that iron was retained on the electrode after use. The phosphorus P 2*p* high resolution spectrum of the electrode after testing was dominated by PO_x species, from the DNA phosphate and possible adventitious adsorption of phosphate from the PBS buffer that the measurement was performed in (Supporting Information, ST22, Fig S18). This developed 2-D sensing platform has high specificity and sensitivity alongwith low limit of detection achieved by PLL-BP nanostructured aptasensor which is superior to all previously reported Mb sensing platforms (see Supporting Information ST21 for comparison to literature).

Conclusions

Surfactant-assisted liquid phase exfoliation of BP nanosheets in aqueous media is reported and PLL was used to functionalise the surface of the nanosheets by non-covalent interactions with the underlying BP to give a PLL modified 2-D material (PLL-BP). An indigenous modified SELEX method for enrichment of DNA aptamers that specifically target and bind the cardiac biomarker Mb was performed. The selected DNA aptamers were bound to PLL-BP by Coulombic interactions. The PLL-BP nanostructured DNA aptasensor was found to be a label-free electrochemical sensing platform for Mb. The direct electron transfer from Mb was measured specifically onto the functionalised PLL-BP-Apt electrodes. The sensor exhibited high specificity and sensitivity imparted by the synergy of high affinity screened aptamers and the enhanced electrochemical properties of the nanoconstruct. The sensor has a very low limit of detection of ~0.524 pg mL^{-1} with a sensitivity of 36 µA pg^{-1} mL cm^{-2} for Mb spiked in serum samples. Our study opens up numerous exciting opportunities to realise better cardiac biomarker detection for point-of-care diagnosis.

ASSOCIATED CONTENT

Supporting Information. Gross appearance of BP colloid, EDX spectra and low voltage EDX, EELS thickness estimation data, optical and SEM characterization of sensor, Raman spectroscopy of PLL-BP, zeta potential measurements, contact angle measurements, liquid chromatography studies, direct electron transfer theory, impedance spectroscopy, electrochemical stability studies, control sensing data, validation of sensor with serum samples, electrochemical response of rGO based sensor, limits of detection of other Mb

sensors in literature, XPS spectrum of sensor post-sensing, DFT calculations of PLL-BP interaction. This material is available free of charge via the Internet at http://pubs.acs.org.

AUTHOR INFORMATION

Corresponding Authors

*To whom correspondence should be addressed:
Prof. Paul O'Brien
Email: paul.o'brien@manchester.ac.uk. Tel: +44 (0)-161 275 4653.
Prof. A. K. Ganguli
Email: ashok@inst.ac.inTel: +91 (0)-172-2210073/75; Fax: +91-172-2210074
Dr. David J. Lewis
Email: david.Lewis-4@manchester.ac.uk Tel: +44 (0)-7940968125
Dr. Priyanka Sabherwal
Email: priyanka@inst.ac.inTel: +91 (0)-172-2210073/75; Fax: +91-172-2210074

†Contributed Equally

ACKNOWLEDGMENT

V. K., G. C. and M. S., H. K. acknowledge INST PDF, CSIR-JRF, and DST, Govt. of India for fellowships. A. K. G. thanks DST, Govt. of India for financial support to INST, Mohali, India. J. B., N. S. and P. O. B. thank the Parker family for funding. P.D.M. is funded by EPSRC (EPSRC grant number EP/K009710/1). L. N., A. P. R., E. A. L. and S. J. H. would like to acknowledge EPSRC grant EP/M010619/1 as well as the defence threat reduction agency grant number HDTRA1-12-1-0013. Some of the equipment used in this study were provided by U. K. Engineering and Physical Sciences Research Council (EPSRC *Core Capability in Chemistry*, EPSRC grant number EP/K039547/1). The authors acknowledge Dr. Suman Singh (CSIR-CSIO, India) for contact angle measurements. The computational facility used in this study was provided by CDAC (Pune, India). Serum samples were provided by Prof. Dr. Manojkumar Rohit, (PGIMER, Chandigarh, India).

REFERENCES

1. Miro, P.; Audiffred, M.; Heine, T., An Atlas of Two-Dimensional Materials. *Chem. Soc. Rev.* **2014,** *43* (18), 6537-6554.

2. Novoselov, K. S.; Geim, A. K.; Morozov, S. V.; Jiang, D.; Katsnelson, M. I.; Grigorieva, I. V.; Dubonos, S. V.; Firsov, A. A., Two-dimensional Gas of Massless Dirac Fermions in Graphene. *Nature* **2005,** *438* (7065), 197-200.

3. Lee, C.; Wei, X.; Kysar, J. W.; Hone, J., Measurement of the Elastic Properties and Intrinsic Strength of Monolayer Graphene. *Science* **2008,** *321* (5887), 385-388.

4. Lee, J.-U.; Yoon, D.; Cheong, H., Estimation of Young's Modulus of Graphene by Raman Spectroscopy. *Nano Lett.* **2012,** *12* (9), 4444-4448.

5. Kuilla, T.; Bhadra, S.; Yao, D.; Kim, N. H.; Bose, S.; Lee, J. H., Recent Advances in Graphene Based Polymer Composites. *Prog. Polym. Sci.* **2010,** *35* (11), 1350-1375.

6. Akhavan, O.; Ghaderi, E.; Rahighi, R., Toward Single DNA Electrochemcial Biosensing by Graphene Nanowalls. *ACS Nano* **2012,** *6*, 2904-2916.

7. Matte, H. S. S. R.; Gomathi, A.; Manna, A. K.; Late, D. J.; Datta, R.; Pati, S. K.; Rao, C. N. R., MoS_2 and WS_2 Analogues of Graphene. *Angew. Chem. Int. Ed.* **2010,** *49* (24), 4059-4062.

8. Wang, Q. H.; Kalantar-Zadeh, K.; Kis, A.; Coleman, J. N.; Strano, M. S., Electronics and Optoelectronics of Two-dimensional Transition Metal Dichalcogenides. *Nat. Nanotechnol.* **2012,** *7* (11), 699-712.

9. Castro Neto, A. H.; Guinea, F.; Peres, N. M. R.; Novoselov, K. S.; Geim, A. K., The Electronic Properties of Graphene. *Rev. Mod. Phys.* **2009,** *81* (1), 109-162.

10. Radisavljevic, B.; Radenovic, A.; Brivio, J.; Giacometti, V.; Kis, A., Single-layer MoS2 Transistors. *Nat. Nanotechnol.* **2011,** *6* (3), 147-150.

11. Liu, H.; Neal, A. T.; Zhu, Z.; Luo, Z.; Xu, X.; Tomanek, D.; Ye, P. D., Phosphorene: An Unexplored 2D Semiconductor with a High Hole Mobility. *ACS Nano* **2014,** *8* (4), 4033-4041.

12. Brent, J. R.; Savjani, N.; Lewis, E. A.; Haigh, S. J.; Lewis, D. J.; O'Brien, P., Production of Few-layer Phosphorene by Liquid Exfoliation of Black Phosphorus. *Chem. Commun.* **2014,** *50* (87), 13338-13341.

13. Kang, J.; Wood, J. D.; Wells, S. A.; Lee, J.-H.; Liu, X.; Chen, K.-S.; Hersam, M. C., Solvent Exfoliation of Electronic-Grade, Two-Dimensional Black Phosphorus. *ACS Nano* **2015,** *9* (4), 3596-3604.

14. Yasaei, P.; Kumar, B.; Foroozan, T.; Wang, C.; Asadi, M.; Tuschel, D.; Indacochea, J. E.; Klie, R. F.; Salehi-Khojin, A., High-Quality Black Phosphorus Atomic Layers by Liquid-Phase Exfoliation. *Adv. Mater.* **2015,** *27* (11), 1887-+.

15. Hanlon, D.; Backes, C.; Doherty, E.; Cucinotta, C. S.; Berner, N. C.; Boland, C.; Lee, K.; Harvey, A.; Lynch, P.; Gholamvand, Z.; Zhang, S.; Wang, K.; Moynihan, G.; Pokle, A.; Ramasse, Q. M.; McEvoy, N.; Blau, W. J.; Wang, J.; Abellan, G.; Hauke, F.; Hirsch, A.; Sanvito, S.; O'Regan, D. D.; Duesberg, G. S.; Nicolosi, V.; Coleman, J. N., Liquid Exfoliation of Solvent-stabilized Few-layer Black Phosphorus for Applications Beyond Electronics. *Nat. Commun.* **2015,** *6*.

16. Fei, R.; Yang, L., Strain-Engineering the Anisotropic Electrical Conductance of Few-Layer Black Phosphorus. *Nano Lett.* **2014,** *14* (5), 2884-2889.

17. Rodin, A. S.; Carvalho, A.; Castro Neto, A. H., Strain-Induced Gap Modification in Black Phosphorus. *Phys. Rev. Lett.* **2014,** *112* (17).

18. Zhu, Z.; Tomanek, D., Semiconducting Layered Blue Phosphorus: A Computational Study. *Phys. Rev. Lett.* **2014,** *112* (17).

19. Li, L.; Yu, Y.; Ye, G. J.; Ge, Q.; Ou, X.; Wu, H.; Feng, D.; Chen, X. H.; Zhang, Y., Black Phosphorus Field-Effect Transistors. *Nat. Nanotechnol.* **2014,** *9* (5), 372-377.

20. *WHO World Health Statistics* **2014,** *(accessed May 12, 2016)*, http://www.who.int/gho/publications/world_health_statistics/2014/en.

21. Nambi, V.; Liu, X.; Chambless, L. E.; de Lemos, J. A.; Virani, S. S.; Agarwal, S.; Boerwinkle, E.; Hoogeveen, R. C.; Aguilar, D.; Astor, B. C.; Srinivas, P. R.; Deswal, A.; Mosley, T. H.; Coresh, J.; Folsom, A. R.; Heiss, G.; Ballantyne, C. M., Troponin T and N-Terminal Pro-B-Type Natriuretic Peptide: A Biomarker Approach to Predict Heart Failure Risk-The Atherosclerosis Risk in Communities Study. *Clin. Chem.* **2013,** *59* (12), 1802-1810.

22. Stillman, A. E.; Oudkerk, M.; Bluemke, D.; Bremerich, J.; Esteves, F. P.; Garcia, E. V.; Gutberlet, M.; Hundley, W. G.; Jerosch-Herold, M.; Kuijpers, D.; Kwong, R. K.; Nagel, E.; Lerakis, S.; Oshinski, J.; Paul, J.-F.; Underwood, R.; Wintersperger, B. J.;

Rees, M. R., Assessment of Acute Myocardial Infarction: Current Status and Recommendations from the North American Society for Cardiovascular Imaging and the European Society of Cardiac Radiology. *Int. J. Cardiovasc. Imaging* **2011,** *27* (1), 7-24.

23. Moreira, F. T. C.; Dutra, R. A. F.; Noronha, J. P. C.; Sales, M. G. F., Electrochemical Biosensor Based on Biomimetic Material for Myoglobin Detection. *Electrochim. Acta* **2013,** *107*, 481-487.

24. Suprun, E.; Bulko, T.; Lisitsa, A.; Gnedenko, O.; Ivanov, A.; Shumyantseva, V.; Archakov, A., Electrochemical Nanobiosensor for Express Diagnosis of Acute Myocardial Infarction in Undiluted Plasma. *Biosens. Bioelectron.* **2010,** *25* (7), 1694-1698.

25. Qureshi, A.; Gurbuz, Y.; Niazi, J. H., Biosensors for Cardiac Biomarkers Detection: A Review. *Sensors Actuators B-Chem.* **2012,** *171*, 62-76.

26. Yang, Z.; Zhou, D. M., Cardiac Markers and Their Point-of-care Testing for Diagnosis of Acute Myocardial Infarction. *Clin. Biochem.* **2006,** *39* (8), 771-780.

27. Priyanka, S.; Shorie, M.; Bhalla, V.; Pathania, P.; Suri, C. R., Nanobioprobe Mediated DNA Aptamers for Explosive Detection. *Chem. Commun.* **2014,** *50* (9), 1080-1082.

28. Wang, L.; Liu, X.; Zhang, Q.; Zhang, C.; Liu, Y.; Tu, K.; Tu, J., Selection of DNA Aptamers that Bind to Four Organophosphorus Pesticides. *Biotechnol. Lett.* **2012,** *34* (5), 869-874.

29. Sabherwal, P.; Mutreja, R.; Suri, C. R., Biofunctionalized Carbon composites: New-generation Diagnostic Tools. *TrAC - Trend. Anal. Chem.* **2016,** *82*, 12-21.

30. Akhavan, O.; Ghaderi, E.; Hashemi, E.; Rahighi, R., Ultra-sensitive Detection of Leukemia by Graphene. *Nanoscale* **2014,** *6*, 14810-14819.

31. Akhavan, O.; Ghaderi, E.; Rahighi, R.; Abdolahad, M., Spongy Graphene Electrode in Electrochemical Detection of Leukemia at Single-cell Levels. *Carbon* **2014,** *79*, 654-663.

32. Holzinger, M.; Le Goff, A.; Cosnier, S., Nanomaterials for Biosensing Applications: A Review. *Front. Chem.* **2014,** *2*.

33. Kumar, V.; Shorie, M.; Ganguli, A. K.; Sabherwal, P., Graphene-CNT Nanohybrid Aptasensor for Label Free Detection of Cardiac Biomarker Myoglobin. *Biosens. Bioelectron.* **2015,** *72*, 56-60.

34. Castellanos-Gomez, A.; Vicarelli, L.; Prada, E.; Island, J. O.; Narasimha-Acharya, K. L.; Blanter, S. I.; Groenendijk, D. J.; Buscema, M.; Steele, G. A.; Alvarez, J. V.; Zandbergen, H. W.; Palacios, J. J.; van der Zant, H. S. J., Isolation and Characterization of Few-layer Black Phosphorus. *2D Mater.* **2014,** *1* (2).

35. Iakoubovskii, K.; Mitsuishi, K.; Nakayama, Y.; Furuya, K., Thickness Measurements with Electron Energy Loss Spectroscopy. *Microsc. Res. Techniq.* **2008,** *71* (8), 626-631.

36. Savjani, N.; Lewis, E. A.; Pattrick, R. A. D.; Haigh, S. J.; O'Brien, P., MoS2 Nanosheet Production by the Direct Exfoliation of Molybdenite Minerals from Several Type-localities. *RSC Adv.* **2014,** *4* (67), 35609-35613.

37. Wang, L.; Sofer, Z.; Pumera, M., Voltammetry of Layered Black Phosphorus: Electrochemistry of Multilayer Phosphorene. *Chemelectrochem* **2015,** *2* (3), 324-327.

38. Tang, L.; Wang, Y.; Li, Y.; Feng, H.; Lu, J.; Li, J., Preparation, Structure, and Electrochemical Properties of Reduced Graphene Sheet Films. *Adv. Func. Mater.* **2009,** *19* (17), 2782-2789.

39. Shumyantseva, V. V.; Sigolaeva, L. V.; Agafonova, L. E.; Bulko, T. V.; Pergushov, D. V.; Schacher, F. H.; Archakov, A. I., Facilitated Biosensing via Direct Electron Transfer of Myoglobin Integrated Into Diblock Copolymer/Multi-walled Carbon nanotube Nanocomposites. *J. Mater. Chem. B* **2015,** *3*, 5467-5477.